JOURNAL OF CATALYSIS 144, 16–29 (1993)

Influence of Coke Deposition on Acidity, Intercrystalline Mass Transfer, and Catalytic Properties of Pt · H–ZSM-5 · Al_2O_3 Catalyst

VASANT R. CHOUDHARY,[1] S. MAYADEVI, AND DEEPAK B. AKOLEKAR

Chemical Engineering Division, National Chemical Laboratory, Pune 411 008, India

Received August 26, 1992; revised May 27, 1993

Influence of coke deposition on Pt · H–ZSM-5 · Al_2O_3 catalyst on its acidity distribution, intercrystalline mass transfer, and catalytic activity/selectivity (in iso-octane cracking, *o*-xylene isomerization and methanol-to-aromatics conversion) has been investigated by carrying out measurements on the catalyst with different extents of coke deposition. The effective intercrystalline diffusivity of iso-octane (which does not penetrate the zeolite channels) in the catalyst at 473 K was measured by the GC pulse technique. The coke deposition has resulted in an increase in the adsorption, apparent heat of adsorption of iso-octane, and xylene isomerization activity, but a decrease in the intercrystalline diffusivity of iso-octane and *para* selectivity in the *o*-xylene isomerization and methanol conversion reactions. The influence of coke deposition (to different extents) on the catalyst on its surface, intercrystalline mass transfer, and catalytic activity/selectivity in the above reactions has been discussed. © 1993 Academic Press, Inc.

INTRODUCTION

Commercial zeolite catalysts are usually available in the form of pellets or extrudates which consist of zeolite crystallites bounded by a binder. The pelletization or extrudation of the zeolite crystallites gives rise to a bimodal pore system for the commercial zeolite catalysts consisting of the micropores in the zeolite and the larger diameter macropores between the crystallites. In commercial zeolite catalyst, in order to minimize intracrystalline mass transfer resistance, small size (<1 μm) zeolite crystals are employed. Though the diffusivities of molecules in the intercrystalline (macro) pores are very much higher than those in the intracrystalline (micro) pores, the diffusion path for intercrystalline mass transfer is very much longer (pellet size >1.5 mm) than that for the intracrystalline mass transfer. Therefore the intercrystalline mass transfer resistance cannot be neglected. The importance of both micro- and macropore diffusion in pelleted zeolite catalysts has been emphasized in the review by Palekar and Rajadhyaksha (*1*). A strong influence of intercrystalline mass transfer on the catalyst activity and selectivity (or product distribution) in the conversion of dimethyl ether to hydrocarbons over ZSM-5 (*2, 3*) and also in the hydrocarbon and alcohol conversion reactions over Pt · H–ZSM-5 · Al_2O_3 (*4*) has been observed earlier.

Carbonaceous deposits (or coke) are inevitable by-products in many acid catalyzed reactions (viz., cracking, isomerization, and alkylation of hydrocarbons, alcohol-to-aromatics conversion, etc.). Though low coke yields are observed for molecular shape-selective zeolites such as ZSM-5, coke deposition on the intercrystalline spaces and pore blockage effects may play a significant role in certain reactions (*5*). Such coke deposition can influence the intercrystalline mass transfer of both the reactants and products through the macropores and change the catalytic activity/selectivity. Influence of coking on intraparticle mass transfer and

[1] To whom correspondence should be addressed.

0021-9517/93 $5.00

catalytic properties, particularly for zeolite catalysts, has not been thoroughly investigated so far.

In our earlier paper (*4*), the influence of intercrystalline mass transfer on catalytic properties of Pt · H–ZSM-5 · Al_2O_3 catalyst has been thoroughly investigated. The present investigation was undertaken with the objective of studying the influence of coking of this catalyst on its acidity distribution, intercrystalline mass transfer, and catalytic activity/selectivity in the iso-octane cracking, *o*-xylene isomerization, and methanol-to-aromatics conversion reactions.

EXPERIMENTAL

The catalyst Pt · H–ZSM-5 · Al_2O_3 (0.1 wt% Pt., 50 wt% Al_2O_3, and for ZSM-5, Si/Al ratio, 70 and crystal size, 0.2–0.3 μm) in the form of 0.16-cm-dia. extrudates was provided by Dr. P. Ratnasamy (National Chemical Laboratory, Pune-8). The catalyst extrudates were made out of a paste containing H–ZSM-5 impregnated (by incipient method) with hexachloroplatinic acid and γ-Al_2O_3 in required amounts, followed by drying at 393 K for 16 h. H–ZSM-5 was prepared by known hydrothermal synthesis of ZSM-5 (U.S. Patent 3702886, 1972) using TPABr as templating agent, removing the template from zeolite channels by its calcination at 823 K for 6 h, repeatedly treating the zeolite with aqueous HCl (0.1 *M*), followed by washing with deionized water and drying at 393 K for 10 h. The catalyst was calcined at 773 K for 4 h and then pretreated at 673 K in a flow of H_2 for 1 h.

The catalyst with different extents of coke deposition was obtained by carrying out cumene cracking reaction at 673 K under differential conditions (i.e., at cumene conversion of less than 10%) for different periods, using 2.5 mol% cumene in nitrogen as the feed. The coked catalyst was heated in a flow of oxygen-free nitrogen at 673 K for 1 h to remove volatile organic material, if any, present in the catalyst. The catalyst poisoned with pyridine was obtained by saturating the uncoked catalyst with pyridine chemisorbed at 523 K.

The coked catalysts were characterized for their surface area by the single-point BET method using a Monosorb Surface Area Meter (Quantachrome, U.S.A.), pore size distribution by mercury porosimetry using an Autoscan-60 porosimeter (Quantachrome, U.S.A.) and carbon content by burning the coke and absorbing completely the carbon dioxide formed in saturated barium hydroxide solution and measuring gravimetrically the barium carbonate formed. (In order to avoid contacting of CO_2 from air with the barium hydroxide solution, N_2 blanketing was used wherever necessary.) Surface analysis of the catalysts was carried out by XPS using a VG-Scientific ESCA-3 MK II electron spectrometer. The thermal analysis data on the catalysts under static air from 298 to 973 K were obtained by using an automatic NETZSCH STA 409 model (Netzsch Geratebau GmbH) thermal analyzer.

The acidity distribution on the catalysts was determined by the step-wise thermal desorption (STD) of pyridine (chemisorbed at 373 K) from 373 to 673 K in a number of temperature steps, using the GC adsorption/desorption method (*6*, *7*). The catalyst (0.2 g) in the column (stainless steel tube with i.d. 2 mm and length 15 cm) was saturated with pyridine at 373 K and the reversibly adsorbed pyridine at this temperature was desorbed in a flow of nitrogen. Pyridine chemisorbed at 373 K was desorbed thermally in the flow of nitrogen by heating the catalyst from 373 and 673 K in six steps (each of 50 K). The temperature in each step was raised at a linear heating rate of 10 K · min^{-1}. After the maximum temperature of the respective step was attained, it was maintained for a period of 1 h to desorb the pyridine reversibly adsorbed on the catalyst at that temperature. The pyridine desorbed at each temperature was measured quantitatively by the detector. The amount of pyridine chemisorbed at 673 K was determined by the pulse technique (*6*). Estimation of the chemisorption data from the STD data is given in an earlier paper (*7*). The chemisorption in the

present study is defined as the amount of pyridine retained by the presaturated catalyst after it has been swept with pure nitrogen for a period of 1 h.

The nature of the coke on the catalyst samples was studied by solid state ^{13}C (CP/MAS) nuclear magnetic resonance spectroscopy at 75.47 MHz on a Bruker MSL 300 FT-NMR spectrometer with a contact time of 4 s and a spinning speed of 4.1 kHz. Dipolar dephasing technique (dephasing delay 40 μs) was employed to distinguish quaternary and methyl carbon. The chemical shifts were measured with respect to adamantine CH carbon taken as 37.8 ppm.

The heat of adsorption of iso-octane on the fresh, coked, and pyridine-poisoned catalyst was determined from the GC pulse technique (*8*) using the relation

$$\log V_R = a - (\Delta H/2.303R)\, 1/T, \quad (1)$$

where V_R is the corrected retention volume of the adsorbate, ΔH is the heat of adsorption, R is the gas constant, T is the temperature, and a is constant.

The effective intercrystalline pore diffusivity of iso-octane (which cannot penetrate the intracrystalline pores of ZSM-5) in the catalysts was determined by the GC pulse method (*8*) based on the van Deemter equation (*9*),

$$\text{HETP} = A + B/v + Cv, \quad (2)$$

where HETP (height equivalent of a theoretical plate) is measured from the chromatogram using the expression (*10*)

$$\text{HETP} = (L/16)\,(y/x)^2. \quad (3)$$

L is the length of the packed column, y is the length of the base line cut by the two tangents of the chromatogram at its points of inflection; and x is the distance from the injection to the peak maximum. The mass transfer term C in Eq. (2) was obtained from the linear plots of HETP versus v at high linear gas velocities (15 to 100 cm $\cdot$ s^{-1}). The effective pore diffusivity, D_p, was estimated from the C term using the following relationships (*9, 11*):

$$C = (F_1 d_p^2 K)/(2\pi^2 F_2 D_p (1 + KF_1/F_2)^2) \quad (4)$$

$$C = F_1F_2(1 + (1 - \varepsilon)/\varepsilon K)\, d_p^2/ 30D_p(1 + F_2(1 - \varepsilon)/\varepsilon K)^2. \quad (5)$$

F_1 and F_2 are the void and solid fractions in the packing, ε is the porosity of the catalyst, and d_p is the average particle diameter. The distribution coefficient K was obtained from the expression (*12*)

$$K = 1/(\varepsilon + (t_m - t_d)vF_1/F_2L), \quad (6)$$

where t_m and t_d are the retention times of the adsorbate and the nonadsorbate, respectively. The retention time of the nonadsorbate was calculated from the knowledge of void space in the column between injector and detector and carrier gas flow rate at the column conditions. The apparent adsorption equilibrium constant K_n was determined from the relation (*13*):

$$K_n = (t_m - t_d)vF_1/L. \quad (7)$$

The GC pulse data required for the heat of adsorption and the effective intercrystalline diffusivity were collected using a Perkin–Elmer Sigma-3B gas chromatograph with flame ionization detector and a stainless steel gc column (i.d. 0.5 cm and length 53 cm) packed with the fresh, coked or poisoned catalyst extrudates (dia. 0.16 cm and length 0.16–0.20 cm). Hydrogen was used as the carrier gas. The concentration of the iso-octane in the pulse was about 1.5 mol% (balance hydrogen) and the pulse size was 0.3 cm^3. In order to carry out measurements at high gas velocities, a part of the gas from the column was bypassed before passing it to the detector.

The activity and selectivity of the catalysts in the iso-octane cracking, *o*-xylene isomerization, and methanol-to-aromatics conversion reactions were determined using a pulse microreactor (stainless steel, o.d. 0.6 cm, i.d. 0.5 cm, length 22 cm) connected to a gas chromatograph. The catalyst (0.2 g) in the microreactor was pretreated *in situ* at 673 K in a flow of H_2 (80 cm^3 $\cdot$ min^{-1}) for 1 h. The catalytic activity was determined

TABLE 1

Carbon Content and Surface Area of Fresh and Coked Pt · H–ZSM-5 · Al_2O_3

Catalyst	wt% of carbon	Vol. of Hg intruded ($cm^3 \cdot g^{-1}$)	Surface area	
			Total ($m^2 \cdot g^{-1}$)	Intercrystalline ($m^2 \cdot g^{-1}$)
Fresh (uncoked) catalyst	0.0	0.53	381	130
Coked catalyst (I)	0.3	0.52	371	121
Coked catalyst (II)	0.4	0.52	368	121
Coked catalyst (III)	2.1	0.51	361	119

using H_2 as carrier gas (flow rate, 80 $cm^3 \cdot min^{-1}$) by injecting a pulse (volume 2.0 μl) of reactant into the reactor at 673 K (pressure 205 kPa) and analyzing the reaction products using a SIGMA-3B GC (column: Bentone-34 (5%) and dinonylphthalate (5%) on chromasorb-w (3 mm × 9 m)) provided with FID and calculating integrator. The details of the microreactor and the procedures for carrying out the reactions and analyzing the reaction products are given earlier (*14, 15*).

RESULTS AND DISCUSSION

Characterization of Uncoked and Coked Pt · H–ZSM-5 · Al_2O_3 Catalysts

Surface area and pore size distribution. The total and intercrystalline surface area (measured by nitrogen adsorption and mercury porosimetry, respectively) and intercrystalline pore volume (obtained from the volume of mercury intruded) for the catalysts coked to different extents are given in Table 1. The results show a small decrease in both the total and intercrystalline surface area of the catalyst due to the coking. The results indicate that at the low coke level, the loss in total surface area is mostly due to a decrease in the intercrystalline surface area, whereas at high coke level the loss is mostly due to a decrease in the intracrystalline surface, probably due to blockage of some of the zeolite channels. The decrease in the intercrystalline pore volume due to the coking is very small. The meso- (present in the alumina particles) and macro- (interparticle and intercrystalline) pore size distribution of the catalyst (*4*) was affected only to a very small extent due to the different levels of coke deposition. The average meso- and macropore radius of the catalysts was found to be 7.0 nm and 0.1 μm, respectively.

Acidity distribution. Temperature dependence of the chemisorption of pyridine on the uncoked and coked catalysts is shown in Fig. 1a. The site energy or acid strength distribution obtained from the STD of pyridine on the catalysts is presented in Fig. 1b. Throughout this paper, the chemisorption is considered as the amount of base retained by the presaturated catalyst after it has been swept with pure nitrogen for a period of 1 h.

It may be noted that the catalysts show a wide acid strength distribution. The acid strength distribution changes considerably with the degree of coking. It is interesting to note that pyridine chemisorption at lower temperatures (<573 K) is increased with increasing coke deposition, whereas at higher temperatures (>650 K), it is decreased with increasing coke deposition (Fig. 1a).

Thermal analysis. The thermal analysis (TG and DTG) of the uncoked and coked catalysts are given in Fig. 2. The DTG curve in Fig. 2c shows a single peak at 373 K due to the desorption of physically adsorbed water from the uncoked catalyst. The DTG curve in Figs. 2a and 2b show a peak at

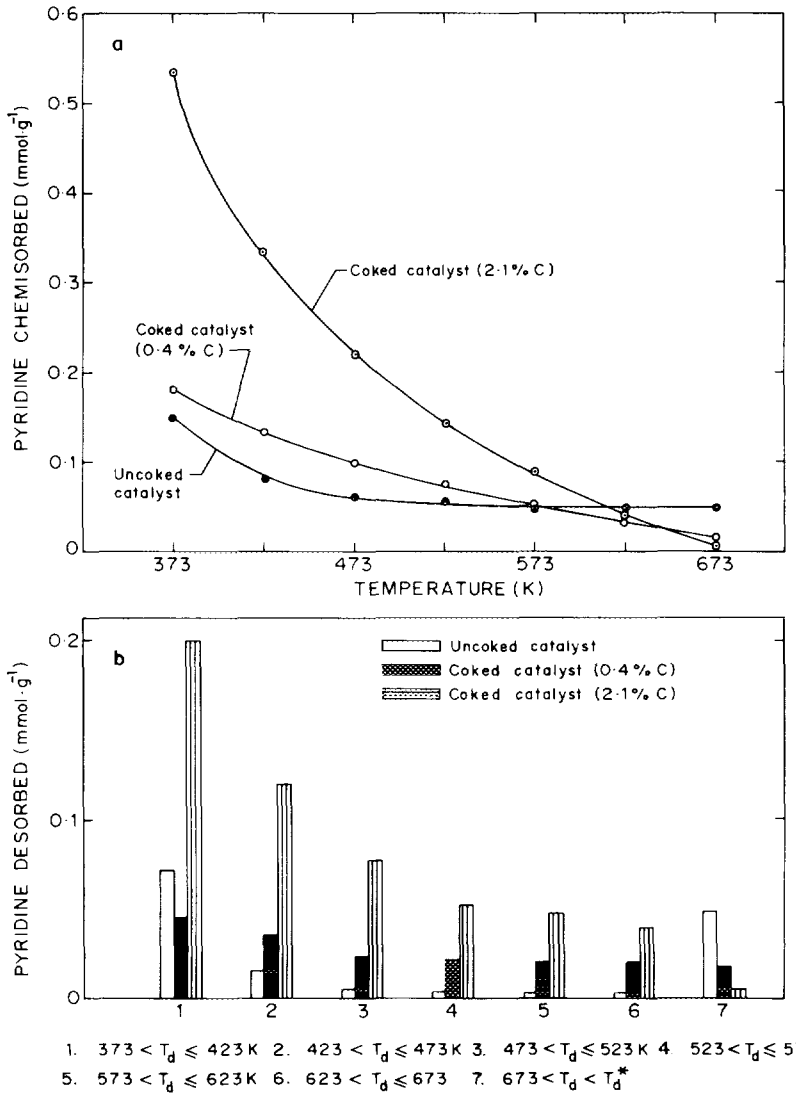

FIG. 1. (a) Temperature dependence of chemisorption of pyridine on Pt · H–ZSM-5 · Al_2O_3 catalyst coked to different extents. (b) Acid strength distribution of the catalyst coked to different extents.

373 K due to the desorption of physically adsorbed water from the coked catalysts and a smaller peak at higher temperature (>730 K). This second peak for the coked catalysts is due to the burning of coke on the catalyst.

For the catalyst with 0.4% carbon, the DTG peak is at 739 K, whereas that for the catalyst with 2.1% carbon is observed at 823 K. This reveals that the removal of coke by its combustion from the catalyst with 2.1% carbon occurs at higher temperature. This indicates that the nature and/or location of the coke in the two coked catalysts is somewhat different. However, the peak temperature shift may also occur if the burning of coke is controlled by oxygen diffusion. Therefore, no firm conclusion can be drawn.

Nature of coke. The XPS (C(1*s*)) spectra of the uncoked and coked catalysts are given

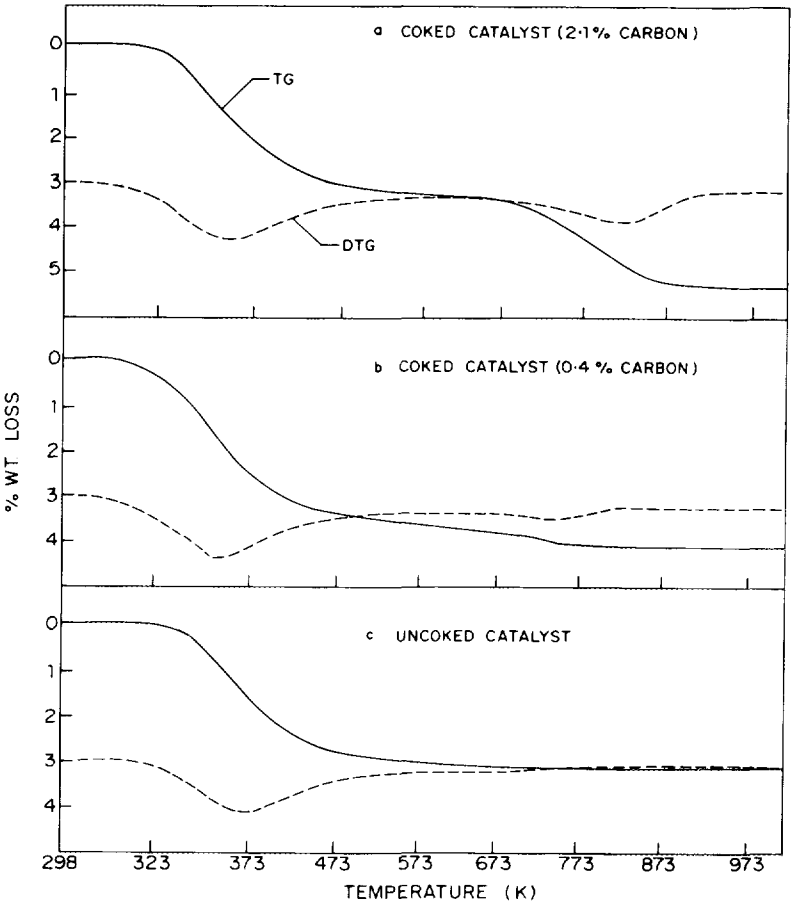

FIG. 2. TG/DTG curves for Pt · H–ZSM -5 · Al_2O_3 catalyst coked to different extents.

in Fig. 3. The C(1*s*) spectrum for the uncoked catalyst is a single sharp peak due to the presence of residual carbon compounds in the spectrometer. For the coked catalyst samples, the C(1*s*) spectrum shows broad and multiple peaks with humps (Fig. 3). Comparison of C(1*s*) spectra of the catalyst coked to different extents reveals that carbon exists in different forms in the coked catalysts and the nature of the coke on the catalyst changes with the extent of coke deposition.

The ^{13}C-CP/MAS NMR spectra of the catalyst coked to different extents are shown in Fig. 4. The ^{13}C-NMR spectrum of the catalyst with 0.4% carbon (Fig. 4a) exhibits three distinct resonances in the range 30–150 ppm which are assigned to (i) secondary, tertiary, and quaternary aliphatic carbons (δ = 30–50 ppm); (ii) aromatic CH groups (δ = 127 ppm); and (iii) substituted aromatic carbons, bridged carbons in condensed aromatics, or olefinic CH groups (δ = 141 ppm) (*16*, *17*). Figure 4b gives the spectrum of the same catalyst sample taken with a dipolar dephasing of 40 μs. Dipolar dephasing technique detects only nonprotonated and methyl carbons. On comparison with Fig. 4a, the signal at 127 ppm is assigned to nonprotonated aromatic carbons and that at 141 ppm is assigned to bridged carbon in condensed aromatics (*16*). The signal at 192 ppm is due to spinning side bands.

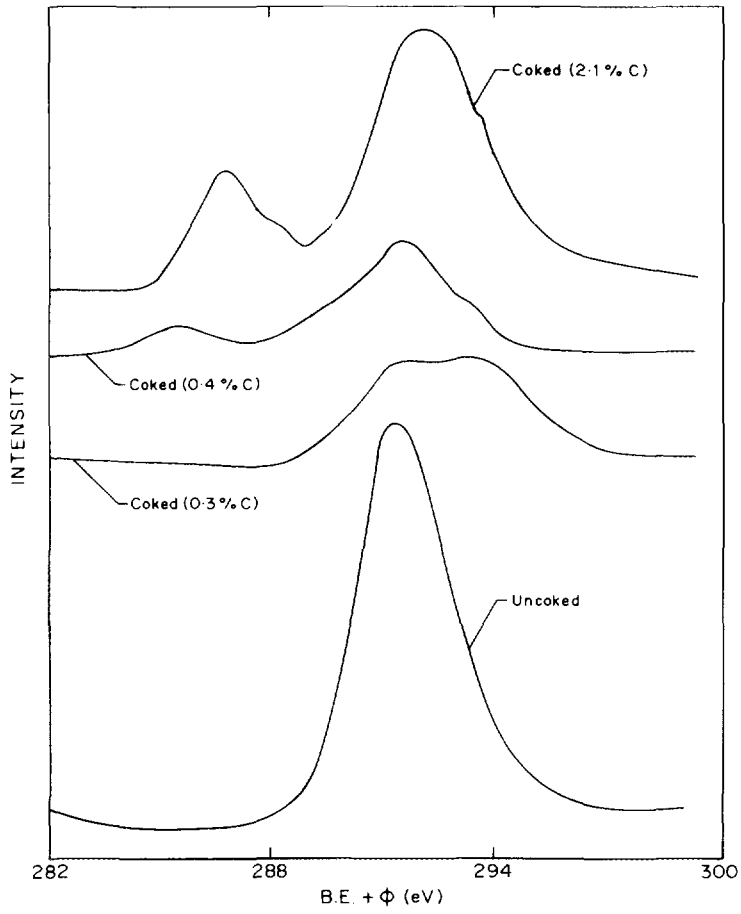

FIG. 3. C(1*s*) spectra of Pt · H–ZSM-5 · Al_2O_3 catalyst coked to different extents (B.E. = binding energy, ϕ = work function).

The ^{13}C-NMR spectrum of the catalyst containing 2.1% carbon (Fig. 4c) gives three signals in the aliphatic range and one signal at 127 ppm in the aromatic range. The signal at 180 ppm is due to spinning side bands. In the aliphatic range, methyl groups attached to secondary carbons (13 ppm), CH_2-groups linked to methyl groups (23 ppm), and other types of paraffinic CH_2-groups and/or quaternary carbon atoms (30–32 ppm) are detected. Figure 4d gives the dipolar dephased spectrum of the same catalyst. The three distinct resonances in the aliphatic range are assigned to (i) methyl groups linked to secondary carbon atoms (13 ppm), (ii) methyl groups linked to aromatics (19 ppm), and (iii) methyl groups linked to aliphatic quaternary carbon (30 ppm). The signal at 127 ppm is assigned to aromatic quaternary carbon and the signal for bridged aromatic carbon is very weak. The results indicate that the NMR visible coke is composed of methyl substituted aromatics, long-chain methyl-substituted aliphatics, and condensed aromatics. Comparison of the spectra for the two coked catalyst samples shows that with the increase in the extent of coke deposition from 0.4 to 2.1%, there is an increase in the ratio of aliphatic to aromatic carbon content of the coke. The polyaromatic or condensed aromatic coke observed on both the catalyst samples is expected to be present only in the meso- and macropores, as the formation of polyar-

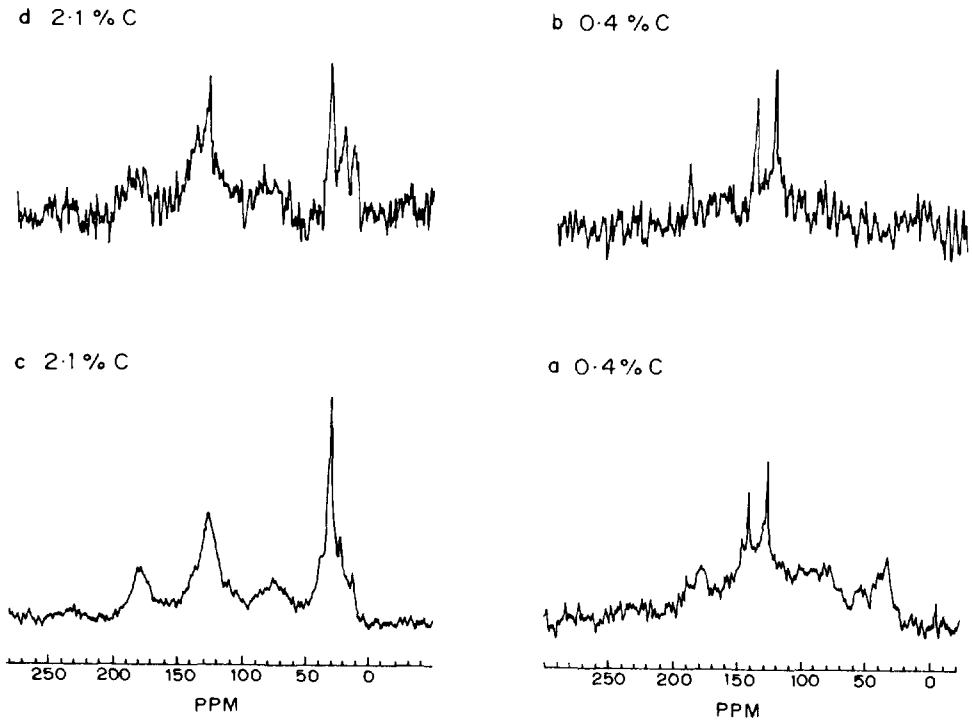

FIG. 4. ^{13}C(CP/MAS) spectra of Pt · H–ZSM-5 · Al_2O_3 catalyst coked to different extents.

omatics is not favored in the channels of ZSM-5 because of restricted transition state molecular shape selectivity of the zeolite (*5, 18*). The aliphatic carbon of the coke is expected to be located in the zeolite channels in the form of strongly sorbed or occluded long chain hydrocarbons and highly alkylated benzenes or polyalkylated benzenes. Earlier studies on pentasil zeolites (*19, 20*) have indicated the deactivation of ZSM-5 in the cumene cracking reaction due to strongly sorbed or occluded hydrocarbons in the zeolite channels. It has also been observed earlier (*15, 21, 22*) that when ZSM-5 zeolite contains a very few strong acid sites or in their absence, the retention of hydrocarbons (mostly in the form of long-chain hydrocarbons) in the zeolite channels is favored during the conversion of alcohols or olefins.

Influence of Poisoning on Adsorption and Mass Transfer

It has been observed earlier (*4*) that the poisoning of Pt · H–ZSM-5 · Al_2O_3 catalyst with pyridine (which can penetrate the macro-, meso-, and micropores of the catalyst) results in a drastic decrease in its activity towards *o*-xylene isomerization and iso-octane cracking reactions. In this study, the influence of poisoning of the catalyst with pyridine (by its chemisorption at 523 K) on the heat of adsorption and diffusion of iso-octane in the catalyst has been investigated. The results are expected to reflect the influence of poisoning of the active sites present in the macro- and mesopores only, as iso-octane cannot penetrate the micropores (intracrystalline pores of ZSM-5) of the catalyst even at 673 K (*19*).

The heats of adsorption of iso-octane on the catalyst with and without the pyridine poisoning estimated from the GC pulse data using Eq. (1) are given in Table 2. The heat of adsorption of iso-octane on the poisoned catalyst is smaller than that on the unpoisoned catalyst. This reveals that the stronger sites (present in the meso- and macropores) involved in the adsorption of iso-octane on the catalyst are blocked due to

TABLE 2

Data on the Adsorption and Mass Transfer of Iso-octane in Pt · H–ZSM-5 · Al_2O_3 Coked to Different Extents and Poisoned by Pyridine

Catalyst	Mass transfer term (at 473 K) C	Distribution coefficient (at 473 K) K	Apparent equil. constant (at 473 K) K_n	Heat of adsorption $-\Delta H$ (kJ · mol^{-1})	Pore diffusivity D_p (cm^2 · s^{-1})	
					From Eq. (4)	From Eq. (5)
Without coking/ poisoning	0.09	0.08	7.2	47.2	2.9	2.5
Poisoned	0.05	0.12	4.6	37.2	7.3	5.4
Coked (0.3% C)	0.09	0.06	9.7	48.1	2.0	1.6
Coked (0.4% C)	0.11	0.05	11.4	53.1	1.5	1.2
Coked (2.1% C)	0.1	0.02	33.1	65.2	0.6	0.5

pyridine poisoning (i.e., due to the chemisorption of pyridine at 523 K).

The mass transfer term C and the intraparticle diffusivity D_p for iso-octane on the unpoisoned and poisoned catalysts have been estimated using Eqs. (2)–(6). Plots of HETP versus linear gas velocity for the estimation of the mass transfer term, C, are given in Fig. 5. The values of the mass transfer term (C), distribution coefficient (K), apparent equilibrium constant (K_n), and effective pore diffusivity (D_p) for the unpoisoned and poisoned catalysts (at 473 K) are included in Table 2. The apparent adsorption equilibrium constant is decreased whereas the intraparticle diffusivity of iso-octane is increased due to the poisoning.

Because of the poisoning, the acid sites

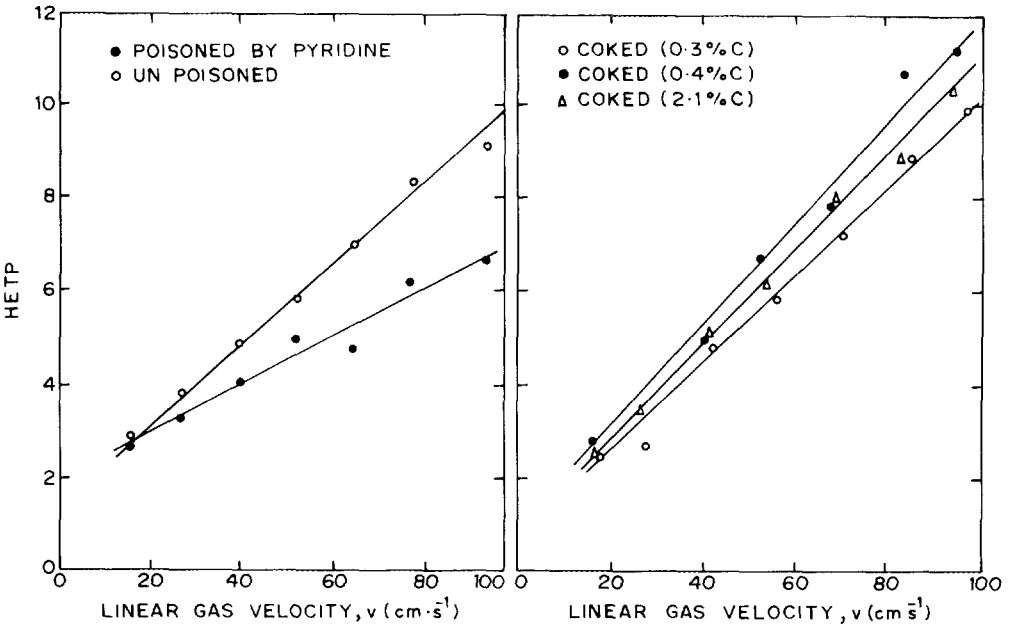

FIG. 5. Plot of HETP vs v of iso-octane on Pt · H–ZSM-5 · Al_2O_3 catalyst with different extents of coke deposition, and poisoned by pyridine.

that are involved in the chemisorption of pyridine at 523 K are blocked and hence are not available for the adsorption of iso-octane. Also, the sites that are available for the adsorption of iso-octane on the poisoned catalyst are weaker. This results in a decrease in both the heat of adsorption and apparent equilibrium constant for the adsorption of iso-octane. Generally, diffusion in porous adsorbent is retarded due to adsorption on the pore walls and is enhanced because of surface diffusion in the adsorbed phase. The observed large increase in the diffusivity of iso-octane in the catalyst due to the poisoning is mostly because of the decreased adsorption of iso-octane. It may also be due to an increase in the surface diffusion because of the decrease in the energy (or heat) of adsorption, which is expected to increase the mobility of adsorbed iso-octane molecules.

Influence of Coking on Adsorption and Mass Transfer

The values of heat of adsorption of iso-octane on the catalyst coked to different extents are included in Table 2. The results reveal that the heat of adsorption and apparent adsorption equilibrium constant of iso-octane on the catalyst increase with increasing the coke content of the catalyst.

The linear plots of HETP versus linear gas velocity for the catalyst with different extents of coke deposition are shown in Fig. 5. The effective pore (meso and macro) diffusivity, D_p, at 473 K has been estimated from the mass transfer term, C, using Eqs. (2)–(6). The values of the adsorption and mass transfer parameters (K_n, K, C, and D_p) are included in Table 2. The effective pore diffusivity decreases with increasing the coke content of the catalyst. The heat of adsorption and the apparent equilibrium constant of iso-octane are increased with increase in the coke deposition indicating an increase in the strength of the acid sites. The increased heat of adsorption of iso-octane is expected to cause retardation in the diffusion of iso-octane in the meso- and macropores of the catalyst. The increased heat of adsorption is also expected to cause a decrease in the surface diffusivity of adsorbed iso-octane.

Influence of Coking on Catalytic Activity

Iso-octane cracking. The data on the activity and selectivity in the iso-octane cracking over the catalyst coked to different extents are presented in Table 3. The iso-octane cracking activity decreases with increasing the extent of coke in the catalyst.

The iso-octane molecules, because of their bulkier size (critical molecular size = 0.7 nm) cannot penetrate the channels of the ZSM-5 zeolite even at 673 K. Hence, the cracking reaction occurs only on the alumina and external surface of the zeolite crystallites. Since iso-octane cracking occurs essentially on strong acid sites (*19, 23*), the decrease in the iso-octane cracking activity of the catalyst with increasing the extent of coke is mostly because of a decrease in the stronger acid sites (in the meso- and macropores) due to the blockage of some of the sites by the coke. The decrease in the iso-octane cracking activity is very much consistent with the decrease in the strong acid sites (measured in terms of the chemisorption of pyridine at 673 K, Fig. 1) on the catalyst due to the coking. The results (Table 3) also show that the formation of aromatics relative to aliphatics (other than iso-octane) is increased with increasing the extent of coke. This may be due to the increased resistance to interparticle or intercrystalline mass transfer due to the coking. The aromatization of the iso-octane cracking products in the zeolite channels is expected to be favored when the intercrystalline mass transfer resistance is increased.

o-Xylene isomerization. The results of *o*-xylene isomerization at 673 K over the catalyst coked to different extents are given in Table 4. The catalyst activity (i.e., conversion of *o*-xylene) passes through a maximum with the increase in the extent of coke deposition. The *p*- to *m*-xylene ratio for the coked catalysts is lower than that for the uncoked

TABLE 3

Data on Cracking of Iso-octane over Pt · H–ZSM-5 · Al_2O_3 Coked to Different Extents

	Uncoked catalyst	Coked catalyst		
		0.3% C	0.4% C	2.1% C
Conversion of iso-octane	44.0	14.0	10.8	9.9
Distribution of hydrocarbons (wt%)				
Iso-octane	56.0	86.0	89.2	90.1
Aliphatics	42.6	11.5	8.3	7.0
Aromatics	1.4	2.5	2.5	2.9
Total	100.0	100.0	100.0	100.0
Aromatics/aliphatics (wt/wt)	0.03	0.22	0.30	0.41

Note. Reaction conditions: Amount of catalyst, 0.2 g; H_2 flow rate, 80 $cm^3 \cdot min^{-1}$; pulse size, 2 μl; pressure, 205 kPa; temperature, 673 K.

catalyst. Both the beneficial and detrimental effects of coke deposition are reflected in the isomerization activity/selectivity presented in Table 4.

An increase in the catalytic activity due to coke deposition has been observed earlier (*24*) for the hydrocarbon conversion reactions on $AlPO_4$–5. Also, earlier studies (*5, 25, 26*) have indicated the possibility of existence of carbonium ion type active sites on coke, which can have both detrimental and beneficial effects on catalytic processes. However, the decrease in the catalytic activity at the higher levels of coke deposition

TABLE 4

Data on Activity and Product Distribution in *o*-Xylene Isomerization over Pt · H–ZSM-5 · Al_2O_3 Coked to Different Extents

	Uncoked catalyst	Coked catalyst		
		0.3% C	0.4% C	2.1% C
Conversion of *o*-xylene	32.0	34.6	41.9	22.8
Distribution of hydrocarbons (wt%)				
Aliphatics	0.5	1.4	5.4	0.8
Benzene	0.1	0.2	0.8	0.1
Toluene	0.9	1.2	3.0	0.6
p-Xylene	13.8	12.9	13.1	7.7
m-Xylene	15.9	18.2	17.7	13.1
o-Xylene	68.6	65.4	58.1	77.2
C_9^+ Aromatics	0.2	0.7	1.9	0.5
Total	100.0	100.0	100.0	100.0
p-X/*m*-X ratio	0.86	0.71	0.74	0.59
Isomerization selectivity	95.3	89.9	73.5	91.2

Note. Reaction conditions: Amount of catalyst, 0.2 g; H_2 flow rate, 80 $cm^3 \cdot min^{-1}$; pulse size, 2 μl; pressure, 205 kPa; temperature, 673 K.

(2.1% carbon) on the catalyst is mostly because of (i) the blockage of some of the zeolite channels by strongly sorbed or occluded hydrocarbon molecules (this is supported by the NMR studies), which makes some of the active sites unavailable/inaccessible to *o*-xylene, and (ii) an increase in the intracrystalline mass transfer resistance for *o*-xylene in the zeolite due to the blockage of some of the zeolite channels by the strongly sorbed or occluded hydrocarbons and also due to the deposition of coke on the external surface of zeolite crystallites, which blocks partially or completely some of the channel openings.

The results (Table 4) show a decrease in the $p - X/m - X$ ratio (i.e., the shape selectivity) due to the coke deposition on the catalyst. This is to be expected because the isomerization reaction occurs to an appreciable extent also on the active sites created due to coke deposition in the meso- and macropores of the catalyst, which is not shape selective. The decrease in the *p*-selectivity may also be attributed to preferential deactivation of the zeolite relative to the deactivation of active sites in the meso- and macropores due to coking.

Methanol-to-aromatics conversion. The influence of coke deposition on the formation of aromatics and their distribution in the conversion of methanol-to-aromatics on the catalyst at 673 K is shown in Table 5. It is very interesting to note that the aromatization in the methanol conversion is strongly influenced by coking; the extent of aromatization decreases drastically with an increase in coke deposition. The distribution of aromatics formed in the methanol conversion reaction is also strongly influenced by the coking. Also, the $p - X/m - X$ ratio is decreased with increasing coke deposition.

The large decrease in the aromatization activity of the catalyst due to the coking is attributed to the decrease in the strong acid sites (measured in terms of chemisorption of pyridine at 673 K) due to coke deposition.

CONCLUSIONS

The following conclusions have been drawn from the present investigation.

1. The poisoning of the Pt · H–ZSM-5 · Al_2O_3 with pyridine (by its chemisorption at 523 K) causes a very significant decrease in the apparent adsorption equilibrium constant and heat of adsorption of iso-octane, but a large increase in its effective diffusivity in the meso- and macropores of the catalyst.

2. The coke deposited on the catalyst is composed of condensed aromatics, methyl-substituted aromatics, and methyl-substituted aliphatics. The ratio of aliphatic-to-aromatic coke increases with increasing the extent of coke deposition. The condensed aromatics are expected to be located in the meso- and macropores, whereas methyl aromatics and aliphatics are expected to be located in the zeolite channels as strongly sorbed or occluded hydrocarbon species.

3. The acidity and acid strength distribution on the catalyst are strongly influenced due to coke deposition.

4. Coke deposition causes a large increase in the adsorption equilibrium constant and heat of adsorption of iso-octane.

5. The effective intercrystalline diffusivity of iso-octane in the coked catalysts is decreased depending upon the extent of coke deposition, mostly as a result of the increased adsorption and heat of adsorption of iso-octane due to the coking.

6. The catalytic activity/selectivity in the iso-octane cracking, *o*-xylene isomerization, and methanol-to-aromatics conversion reactions is strongly influenced by the coke deposition. When the extent of coke on the catalyst is increased, (i) the iso-octane cracking activity is decreased due to deactivation of intercrystalline strong acid sites, (ii) the xylene isomerization activity is initially increased (for lower coke deposition) and then decreased (for higher coke deposition), (iii) the extent of aromatization in the methanol-to-aromatics conversion is decreased due to the deactivation and/or blockage of strong acid sites, and (iv) the

TABLE 5

Data on Activity and Product Distribution in Methanol-to-Aromatics Conversion on Pt · H–ZSM-5 · Al_2O_3 Coked to Different Extents

	Uncoked catalyst	Coked catalyst		
		0.3% C	0.4% C	2.1% C
Conversion of methanol (%)	100.0	100.0	100.0	100.0
Concentration of aromatics in the hydrocarbons (%)	21.0	12.0	10.7	5.2
Distribution of aromatics (wt%)				
Benzene	2.1	5.0	11.2	11.7
Toluene	9.1	7.5	9.3	19.4
Ethyl benzene	2.9	1.7	1.9	3.9
p-Xylene	16.9	18.3	15.0	12.6
m-Xylene	19.0	21.7	18.7	17.9
o-Xylene	15.0	13.3	15.0	15.1
(Total xylenes)	(50.9)	(53.3)	(48.7)	(45.6)
C_9^+ Aromatics	35.0	32.5	28.9	19.4
Total	100.0	100.0	100.0	100.0
p-X/*m*-X ratio	0.89	0.84	0.80	0.70

Note. Reaction conditions: Amount of catalyst, 0.2 g; H_2 flow rate, 80 $cm^3 \cdot min^{-1}$; pulse size, 2 μl; pressure, 205 kPa; temperature, 673 K.

para selectivity in *o*-xylene isomerization and alcohol conversion reactions is decreased because of the occurrence of xylene isomerization, to an appreciable extent, in the meso- and macropores (which is not shape selective).

ACKNOWLEDGMENTS

The authors are grateful to Dr. P. Ratnasamy for providing the catalyst sample, Dr. V. G. Gunjikar and Dr. S. Badrinarayan for their assistance in thermal analysis and XPS, and Dr. S. Ganapathy and Dr. P. R. Rajamohanan for their help in MAS-NMR studies.

REFERENCES

1. Palekar, M. G., and Rajadhyaksha, R. A., *Catal. Rev.-Sci. Eng.* **28,** 371 (1986).
2. Doelle, H. J., Heering, J., Riekert, L., and Marosi, L., *J. Catal.* **71,** 27 (1980).
3. Heering, J., Kotter, M., and Riekert, L., *Chem. Eng. Sci.* **37,** 581 (1982).
4. Choudhary, V. R., and Akolekar, D. B., *J. Catal.* **116,** 130 (1989).
5. Derouane, E. G., *in* "Catalysis by Acids and Bases" (B. Imelik *et al.*, Eds.), p. 221. Elsevier, Amsterdam, 1985.
6. Choudhary, V. R., and Nayak, V. S., *Appl. Catal.* **4,** 31 (1982).
7. Choudhary, V. R., *J. Chromatogr.* **268,** 207 (1983); Nayak, V. S. and Choudhary, V. R., *J. Catal.* **81,** 26 (1983).
8. Choudhary, V. R., and Doraiswamy, L. K., *Ind. Eng. Chem. Prod. Res. Dev.* **10,** 218 (1971).
9. van Deemter, J. J., Zuiderweg, F. J., and Kinkenberg, A., *Chem. Eng. Sci.* **5,** 271 (1956).
10. McNair, H. M., and Bonelli, E. J., "Basic Gas Chromatography," Varian Instruments Division, California, 1969.
11. Hawkes, S. J., *J. Chromatogr.* **68,** 1 (1972).
12. Eberly, P. E., Jr., *Ind. Eng. Chem. Fundam.* **8,** 25 (1969).
13. Eberly, P. E., Jr., and Spencer, E. M., *Trans. Faraday Soc.* **56,** 289 (1961).
14. Nayak, V. S., and Choudhary, V. R., *Appl. Catal.* **4,** 333 (1982).
15. Nayak, V. S., and Choudhary, V. R., *J. Catal.* **81,** 26 (1983).
16. Weitkamp, J., and Maxiner, S., *Zeolites* **7,** 6 (1987).
17. Carlton, L., Copperthwaite, R. G., Hutchings, G. J., and Reynhardt, E. C., *J. Chem. Soc. Chem. Commun.*, 1008 (1986).
18. Dejaifve, P., Auroux, A., Gravelle, P. C., Vedrine, J. C., Gabelica, Z., and Derouane, E. G., *J. Catal.* **70,** 123 (1981).

19. Choudhary, V. R., and Akolekar, D. B., *J. Catal.* **125,** 143 (1990).
20. Akolekar, D. B., and Choudhary, V. R., *J. Catal.* **105,** 416 (1987).
21. Nayak, V. S., and Choudhary, V. R., *Appl. Catal.* **9,** 251 (1984).
22. Choudhary, V. R., and Nayak, V. S., *Zeolites* **5,** 325 (1985).
23. Choudhary, V. R., *Zeolites* **7,** 272 (1987).
24. Choudhary, V. R., and Akolekar, D. B., *J. Catal.* **103,** 115 (1987).
25. Echigoya, E., Sano, H., and Tanaka, M., *in* "Proceedings, 8th International Congress on Catalysis, Berlin, 1984, p. V-623. Dechema, Frankfurt-am-Main, 1984.
26. Menon, P. G., *J. Mol. Catal.* **59,** 207 (1990).